Aug 24th, 12:00 AM - Aug 25th, 12:00 AM

Self-shape Optimisation of Cold-formed Steel Columns

Benoit P. Gilbert

Timothee J-M Savoyat

Lip H. The

Twenty-First International Specialty Conference on Cold-Formed Steel Structures
St. Louis, Missouri, USA, October 24 & 25, 2012

Self-shape optimisation of cold-formed steel columns

Benoit. P. Gilbert[1], Timothee J.-M. Savoyat[2] and Lip H. Teh[3]

Abstract

This paper presents the optimisation of cold-formed steel open columns using the recently developed self-shape optimisation method that aims to discover new profile shapes. The strength of the cold-formed steel sections is calculated using the Direct Strength Method, and the rules developed in the present work to automatically determine the local and distortional elastic buckling stresses from the Finite Strip and constrained Finite Strip Methods are discussed. The rules are verified against conventional and optimum sections yielded in this research, and found to accurately predict the elastic buckling stresses. The principles behind the self-shape optimisation method are summarised herein and are applied to singly-symmetric (mono-symmetric) cold-formed steel columns. "Optimum" cross-sections for simply supported columns, 0.047 inch (1.2 mm) thick, free to warp and subjected to a compressive axial load of 11,167 lb (75 kN) are presented for column lengths ranging from 39.37 inches to 98.42 inches (1,000 mm to 2,500 mm). Results show that the optimum cross-sections are found in a relatively low number of generations, and typically shape to non-conventional "bean", "oval" or rounded "Σ" sections. The algorithm optimises for distortional and global buckling, therefore likely subjecting the cross-sections to buckling interaction.

Introduction

Cold-formed steel columns are widely used in the construction industry due to their lightweight, easy installation and erection, and economy. The strength and

[1] Lecturer, Griffith University, Gold Coast, Australia,
[2] Former exchange undergraduate student, Griffith University, Gold Coast, Australia
[3] Senior Lecturer, University of Wollongong, Wollongong, Australia

efficiency of cold-formed steel profiles depends on the cross-sectional shape, which controls the three fundamental buckling modes: local, distortional and global. Despite the manufacturing process allowing achievement of almost any desired cross-sections, only conventional C, Z or Σ cross-sectional shapes are normally used in practice.

Research involving optimisation of un-predefined cross-sections have been carried out successfully by Griffiths and Miles (2003) for hot-rolled steel profiles and Liu et. al. (2004) for cold-formed steel profile. Griffiths and Miles (2003) used Genetic Algorithm (GA) and a voxel-based representation in which the design space was decomposed into a grid of identical sized squares. Liu et al. (2004) used a "knowledge-based global optimisation" which found promising cross-sections through the knowledge-based optimisation process, and further optimised using a gradient-based local optimisation process. The sections were limited to eight folds, and minor stiffeners adding strength to the profiles were not considered.

Recently, Leng et al (2011) optimised the cross-sectional shapes of cold-formed steel open columns using three different optimisation algorithms. Sections having a wall thickness of 0.039 inch (1 mm) and a perimeter of 11.02 inches (280 mm) were divided into 21 elements, and optimum "open circular" and "S" cross-sections were found. Similar to Liu et al. (2004), the length of the elements (about 14 times the profile thickness) may not allow small bending radii in the cross-sections and minor stiffeners to be created.

This paper aims to strength optimise cold-formed steel columns using the self-shape optimisation principles detailed in Gilbert et. al. (2011) by introducing the Direct Strength Method (DSM) in the algorithm.

Automatic determination of the elastic buckling stresses of cold-formed steel profiles for optimisation purposes is challenging as "engineering judgement" is often needed to select the appropriate buckling value when elastic buckling analyses fail to directly identify a mode. This paper presents a clear set of rules to obtain the local and distortional elastic buckling stresses using the Finite Strip Method (FSM) (Cheung, 1976) and constrained Finite Strip Method (cFSM) (Adany and Schafer, 2006, 2008). The rules are verified against conventional and "optimum" cross-sections yielded in the present work, and are found to accurately predict the elastic buckling stresses. The operators behind the self-shape optimisation principles that allow the cross-section to self-shape to an "optimum" profile are summarised for singly-symmetric (mono-symmetric) open cross-sections, and columns of lengths varying from 39.37 inches (1,000 mm) to 98.42 inches (2,500 mm) are optimised for a targeted compressive axial

capacity of 16,861 lb (75 kN). The optimum cross-sectional shapes found in the present work are discussed with respect to their shape, dimensions, critical buckling modes and buckling mode interactions.

Optimisation problem

The present optimisation problem is illustrated in Figure 1 and is concerned with minimising the cross-sectional area A of a column subjected to an axial compressive load N^* of 16,861 lb (75 kN). The column is composed of 0.047 inch (1.2 mm) thick cold-formed steel open section, and is free to warp at the supports. The yield stress f_y is 65.3 ksi (450 MPa), the Young modulus E is 29,007 ksi (200 GPa) and the shear modulus G is 11,167 ksi (77 GPa). Buckling lengths ranging from 39.37 inches (1,000 mm) to 98.42 inches (2,500 mm), in 19.69 inches (500 mm) increment, are included in the present study.

The unconstrained optimisation problem suitable for GA consists of minimising the "fitness function" f, composed of the objective and penalty functions, as,

$$\text{Minimise } f = \frac{A}{A_{squash}} + \alpha \left| \frac{N^*}{N_c} - 1 \right| \tag{1}$$

where N_c represents the nominal axial capacity of the column, the parameter α is a penalty factor associated with the penalty function, and A_{squash} represents the lower bound cross-sectional area of the profile, defined as,

$$A_{squash} = N^* / f_y \tag{2}$$

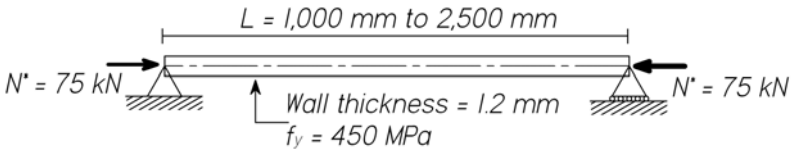

Figure 1 : Optimisation of an open thin-walled section column

Automatic determination of the nominal axial compression capacity N_c

The Direct Strength Method for columns

In order to estimate the nominal axial compression capacity N_c of the column in Eq. (1), the Australian design standard AS/NZS 4600 Cold-formed Steel Structures (AS/NZS 4600, 2005) is used in the present work. The standard

allows the determination of the axial capacity using two distinct methods, referred to as the "Effective Width Method" (EWM) and the "Direct Strength Method" (DSM). The DSM, developed by Schafer and Pekoz (1998), looks at the entire member rather than individual elements as in the EWM and has the advantages of offering the same design simplicity for complex and simple sections. Its recent development for the design of cold-formed steel sections (AISI, 2006, Schafer, 2006) has simplified the design procedure when compared to earlier methods based on the EWM (Hancock, 2007). More importantly, it allows a more direct route to section optimisation as the three fundamental buckling modes (local, distortional, and global) are now represented by direct strength equations thus allowing the GA to operate with a more clearly defined set of constraints. In the DSM, the global, local and distortional axial member capacities, N_{ce}, N_{cl} and N_{cd}, respectively, are determined, and the nominal member capacity in compression N_c is equal to the lowest of them (see AISI (2006) for more details),

$$N_c = min\left(N_{ce}, N_{cl}, N_{cd}\right) \tag{3}$$

Elastic buckling stresses

In the DSM, the elastic global, local and distortional buckling stresses f_{oc}, f_{ol} and f_{od}, respectively, are needed to calculate the global, local and distortional member capacities N_{ce}, N_{cl} and N_{cd}, respectively. The elastic global buckling stress f_{oc} can be estimated by either the Finite Strip Method (FSM) or Timoshenko's buckling theory, whereas the elastic local and distortional buckling stresses f_{ol} and f_{od} are typically estimated using the FSM. A Finite Strip analysis provides a buckling curve, also referred to as the "signature curve", of the buckling stresses against the half-wavelength with the associated buckling modes. Ideally, a buckling curve has two minima corresponding to the elastic local (first minimum) and distortional (second minimum) buckling stresses. However, Finite Strip analyses often result in one or no local minimum, and fail to directly identify the local and/or distortional buckling stresses. Indistinct buckling modes can be manually identified as discussed in AISI (2006) and Section "Validation of the proposed rules". Yet, the recent development of the constrained Finite Strip Method (cFSM) (Adany and Schafer, 2006, 2008) opened new possibilities in optimisation of cold-formed steel members by providing automatic identification of indistinct buckling modes (Schafer, 2008). The cFSM enables calculations of "pure" buckling modes and separates buckling modes into four subspaces referred to as "global", "distortional", "local" and "other".

Currently, no clear set of proven rules exists to automatically determine the local and distortional elastic buckling stresses for shape optimisation. For general

optimisation purposes, Schafer (2008) recommends the use of the cFSM to determine the critical half-wavelengths from the "pure" modes (i.e. determining the half-wavelengths corresponding to the minimum of the "pure" mode buckling curves) in conjunction with the use of FSM to determine the buckling stresses. Additionally, Li and Shafer (2010a) advises to perform constrained Finite Strip analyses on straight-line models, ignoring the corners. The latter recommendation is however not suitable for shape optimisation purposes that typically generate rounded cross-sections, as shown in Section "Results" and Leng et. al. (2011). Alternatively, if the signature curve from a Finite Strip analysis has unique minima, the need for performing a constrained Finite Strip analysis may be avoided (Li and Schafer, 2010a).

For shape optimisation purposes, Leng et. al. (2011) only performed Finite Strip analyses and, if more than one local minimum exist on the buckling curve, chose the first local minimum of the buckling curve for f_{ol} and the smallest of the remaining local minima, for f_{od}. If only one local minimum exists, then this minimum is chosen for f_{ol} if it occurs at a half-wavelength less than a reference length. Otherwise, the local minimum is chosen for f_{od}. The reference half-wavelength is initially taken as the "perimeter length" and regularly updated through the optimisation process as the distortional critical half-wavelength when more than one local minimum exists. However, it is not clear if the method consistently determines the actual elastic buckling stresses, as if only one local minimum exists and is greater than the reference length, the algorithm is likely to overestimate the critical half-wavelength L_{crl} for local buckling. Conversely, if the local minimum occurs at a half-wavelength less than the reference, the critical half-wavelength L_{crd} for distortional buckling may be underestimated.

The use of the cFSM for local buckling and shape optimisation

The calculation of the "pure" local buckling curve from the cFSM requires intermediate nodes, referred to as "sub-nodes", to be inserted between "main nodes". The main nodes are located at the intersection of two strips having a non-zero angle relative to each other (Adany and Schafer, 2008). Consecutive sub-nodes are therefore aligned and the plates are only able to buckle between main nodes. Consequently, the cFSM for local buckling is well suited for cross-sections with straight lines and no rounded corners. For randomly drawn cross-sections where strips are likely to have non-zero angles relative to each other or for cross-sections with not perfectly flat sides, it is unclear which nodes have to be considered as sub-nodes. Moreover, it is likely that the transition from a sub-node to a main node is a gradual process, with sub-nodes partially preventing the plate to buckle between main nodes.

Currently, Finite Strip analysis programs, such CUFSM (Li and Schafer, 2010b) used in this study, checks if three or more consecutive nodes are aligned, within a given tolerance, to make the distinction between sub-nodes and main nodes, and is likely to consider too many nodes as main nodes in the current optimisation process, give low critical half-wavelengths and therefore overestimate the local elastic buckling stress f_{ol}. This statement is illustrated in Savoyat et. al. (2012) using two lipped Cee sections with one having misaligned nodes in the web by half the profile thickness. Finite Strip analyses of the two cross-sections show little difference in the buckling curve and both cross-sections have the same critical half-wavelength L_{crl} for local buckling. However, a constrained Finite Strip analysis predicts different half-wavelength for the two cross-sections, resulting in the overestimation of the elastic local buckling stress by 50% for the "misaligned" cross-section. Determining the critical local half-wavelength using cFSM is therefore not recommended for arbitrarily drawn or rounded cross-sections that have node misalignments, and the recommendation in Li and Schafer (2010a) and Schafer (2008) described in the previous section cannot be used for local buckling and shape optimisation.

Proposed rule for determining the elastic local buckling stress f_{ol}

The critical half-wavelength L_{crl} for local buckling for a member in compression is typically less than or equal to the largest outside dimension d of the cross-section (AISI, 2006), and the elastic local buckling stress f_{ol} would typically correspond to the minimum of the buckling curve at a half-wavelength lower than d. Therefore, following this observation, the elastic local buckling stress f_{ol} of a cross-section is determined from the smallest local minimum, if it exists, or from the smallest gradient of the buckling curve, in the half-wavelength interval $[r_0, d]$, where r_0 is the least radius of gyration of the column.

Proposed rule for determining the elastic distortional buckling stress f_{od}

Distortional buckling occurs at a half-wavelength significantly greater than local buckling, typically between three and nine times the largest outside dimension d of the cross-section (AISI, 2006). Stub column tests do not generally pick up distortional buckling (Hancock, 1985), and AS/NZS 4600 (2005) recommends a maximum length for stub-column tests of twenty times the least radius of gyration r_0. Therefore, the literature shows that distortional buckling likely occurs at a half-wavelength between the lesser of $20r_0$ and $3d$, and $9d$. However, verification of the present rules in Section "Validation of the proposed rules" showed that a value of 10d is a better upper limit for distortional buckling, and is adopted herein. Following these observations and the recommendations by

Schafer (2008) discussed previously, the half-wavelength L_{crd} for distortional buckling is determined using the cFSM in the half-wavelength interval [min ($20r_0$, $3d$), $10d$], and the elastic buckling stress is then determined using the FSM. If more than one local minimum exist on the "pure" distortional buckling curve, the half-wavelength for distortional buckling is taken at the smallest local minimum.

Validation of the proposed rules

The proposed set of rules for determining the elastic local and distortional buckling stresses is validated in this section against a manual method, subjected to engineering judgement and best practice for handling indistinct buckling modes, as discussed in AISI (2006). If indistinct local mode occurs, options to determine the critical local half-wavelength L_{crl} include: (i) refining the half-wavelengths, (ii) basing judgement on the definition of the buckling mode given in AISI (2006), or (iii) if possible, pin internal fold lines to force local buckling. Similarly, if indistinct distortional mode occurs, options to determine the critical local half-wavelength L_{crd} include: (i) refining the half-wavelengths, (ii) basing judgement on the definition of the buckling mode given in AISI (2006), (iii) slightly varying the dimensions of the model to recognise a trend in distortional buckling minima or (iv) if possible, pin appropriate internal fold lines to force distortional buckling.

Forty eight conventional cross-sections and twelve "optimum" cross-sections, found in Section "Results", are used to validate and cross-validate, respectively, the proposed set of rules. Specifically, the following cross-sections are considered:

- 16 lipped Cee-sections and 16 lipped Zed-sections commonly used in Australia and manufactured by BlueScope Steel Lysaght (BlueScope Lysaght, 2009). The nominal depth of the profiles ranges from 3.93 inches (100 mm) to 13.78 inches (350 mm), and the nominal wall thickness from 0.039 inch (1.0 mm) to 0.12 inch (3.0 mm).
- 16 typical storage rack uprights, with nominal depth ranging from 2.16 inches (55 mm) to 4.33 inches (110 mm), and nominal wall thickness ranging from 0.047 inch (1.2 mm) to 0.094 inch (2.4 mm). See Savoyat et. al. (2012) for more details on the profiles.
- 12 "optimum" cross-sections found in Section "Results", corresponding to the three fittest cross-sections for each of the four column lengths investigated.

Table 1 shows the average difference in determining the local and distortional elastic buckling stresses from the manual method and automated set of rules. Detailed results can be found in Savoyat et. al. (2012). Table 1 shows that the two methods give similar results, with an average difference of less than 1% for all cross-sections analysed and for the two modes of buckling. The maximum difference is equal to 8.6% and is encountered for a 2.16 inches (55 mm) deep and 0.094 inch (2.4 mm) thick storage rack upright. The standard deviation in predicting the elastic buckling stresses between the two methods is equal to 1.6% and 1.9% for the local and distortional buckling, respectively.

	Nb. of section	Difference in elastic buckling stresses relative to the manual method (%)[(1)]					
		Local			Distortional		
Section type	analysed	Average	Min	Max	Average	Min	Max
Cee	16	0.0	0.0	0.0	0.6	0.0	2.2
Zed	16	0.0	0.0	0.0	0.6	0.0	3.8
Rack uprights	16	-0.8	-8.6	0.0	-1.6	-8.1	0.0
Optimum	12	0.7	-2.1	4.7	0.7	0.0	2.6
All	60	-0.08	--	--	0.03	--	--

(1) *A negative percentage value means that the automated set of rules provides a lower elastic stress than the manual method*

Table 1: Comparison between manual method and automated rules

Self-shape optimisation principles

The self shape optimisation method enables a cross-section to shape to an optimum by using the evolution and adaptation benefits of Genetic Algorithm (Holland, 1975). The general principles are detailed in Gilbert et. al. (2011) and in Savoyat et. al. (2012) for the particular case of singly-symmetric cross-sections. The feasibility and accuracy of the method have been verified by implementing it to optimise the section capacity of thin-walled profiles. Specifically, the profiles were optimised against simple parameters for which analytical solutions are known, i.e. minimising the cross-sectional area of doubly symmetric thin-walled profiles for imposed second moments of area about the two axes of symmetry.

The optimisation method is believed to significantly reduce computational time and allow cross-sections to be drawn with element sizes comparable to wall thickness, therefore enabling small stiffeners to be considered in the optimisation process. Moreover, the specificity of the operators described in the following points allows the algorithm to converge in a relatively low number of

generations (less than 100 generations). The principles of the method are summarised below for singly-symmetric profiles:

- A floating-point type GA is used in the self-shape optimisation method, meaning a cross-section is not defined using typical binary strings, but by floating-point numbers representing the coordinates of the points constituting the cross-section.
- The initial population in GA is generated by arbitrarily drawing cross-sections using self-avoiding random walks. The self-avoiding random walks enable the creation of cross-sections without presumptions on their shapes, and allow the creation of continuous and smoothly curved cross-sectional shapes. Figure 2 shows examples of initial cross-sections for half of singly-symmetric cross-sections on a 3.94 inches × 3.94 inches (100 mm × 100 mm) design space. The horizontal axis $x = 0$ is the axis of symmetry. Small stiffeners can be created by using an element length in the order of magnitude of the profile thickness, as evident in Figure 2.
- Cross-over and mutation operators are performed in relation to the design space and not to the floating-point variables as in traditional GA. The cross-over operator allows for the merging of two cross-sections to generate offsprings bearing similarity in cross-sectional shapes to the two parents. In the mutation operator, a part of the cross-section is deleted and redrawn (Gilbert, et al., 2011, Savoyat, et al., 2012).

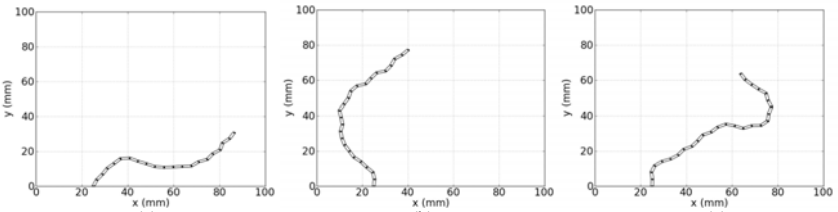

(a) (b) (c)

Figure 2: Example of initial cross-sections on a 100 mm × 100 mm design space of (a) 41 elements, (b) 49 elements and (c) 53 elements

In the present work, a design space of 3.94 inches × 3.94 inches (100 mm × 100 mm) is used in generating the half cross-sections for the singly-symmetric cross-sections. A nominal element size of 4 mm (i.e. 3.33 times the thickness) is used and found to be a reasonable compromise between accuracy of the cross-sectional area (by allowing complex cross-sectional shapes, including stiffeners, to be drawn) and computational time. The augmented Lagrangian method for GA described in Adeli and Cheng (1994) is used herein to improve converge.

Results

This section presents the "optimum" singly-symmetric open cross-sections obtained for the 39.37 inches, 59.05 inches, 78.74 inches and 98.42 inches (1,000 mm, 1,500 mm, 2,000 mm and 2,500 mm) long columns. For each column length, 10 runs were performed with an initial population of 500 individuals. A maximum of 80 generations were analysed per run.

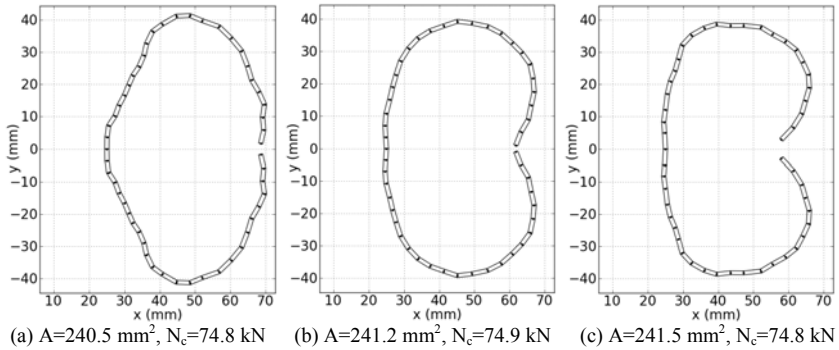

(a) A=240.5 mm^2, N_c=74.8 kN (b) A=241.2 mm^2, N_c=74.9 kN (c) A=241.5 mm^2, N_c=74.8 kN

Figure 3: "Optimum" cross-sections for a column length of 1,000 mm, (a) fittest cross-section, (b) second fittest cross-section and (c) third fittest cross-section

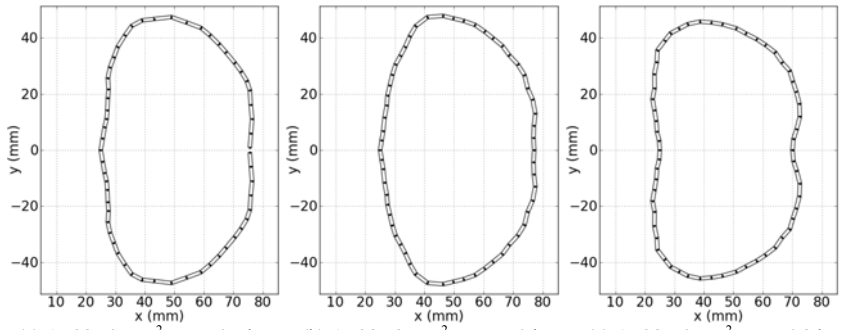

(a) A=287.2 mm^2, N_c=74.7 kN (b) A=287.8 mm^2, N_c=75.0 kN (c) A=287.6 mm^2, N_c=74.8 kN

Figure 4: "Optimum" cross-sections for a column length of 1,500 mm, (a) fittest cross-section, (b) second fittest cross-section and (c) third fittest cross-section

Figure 3 through Figure 6 plot the three fittest cross-sections out of the 10 runs at the 80th generation for the 39.37 inches, 59.05 inches, 78.74 inches and 98.42 inches (1,000 mm, 1,500 mm, 2,000 mm and 2,500 mm) long columns, respectively. The fitness *f* of the cross-sections is evaluated using Eq. (1) with a penalty factor α of 1.0. The entire design space is not plotted in Figure 3 through

Figure 6 for clarity. All cross-sections found in this study are given in Savoyat et. al. (2012).

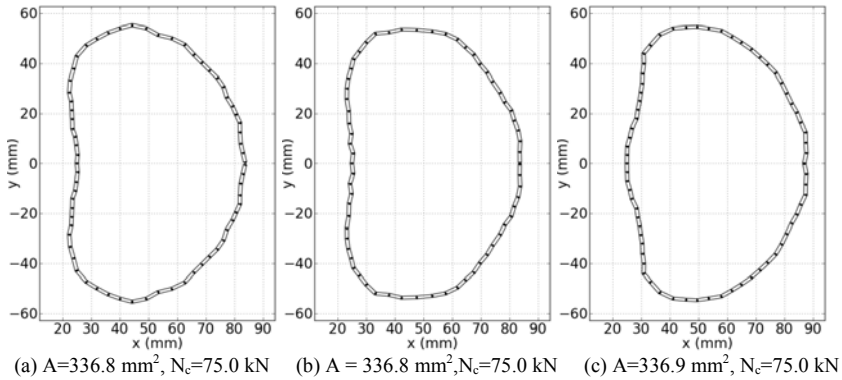

(a) A=336.8 mm^2, N_c=75.0 kN (b) A = 336.8 mm^2,N_c=75.0 kN (c) A=336.9 mm^2, N_c=75.0 kN

Figure 5: "Optimum" cross-sections for a column length of 2,000 mm, (a) fittest cross-section, (b) second fittest cross-section, and (c) third fittest cross-section

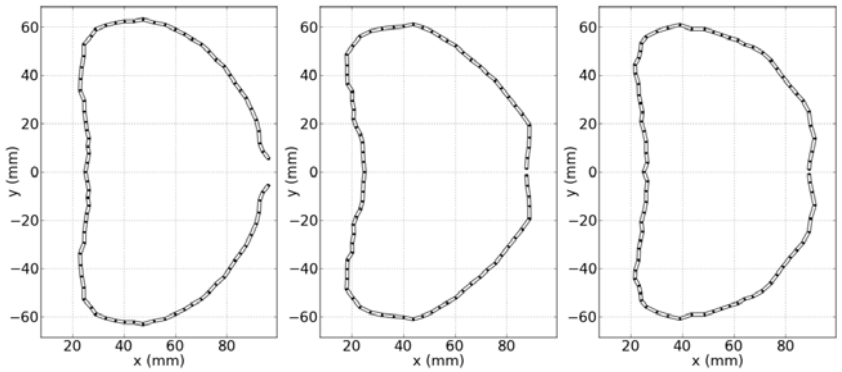

(a) A=385.8 mm^2, N_c=74.9 kN (b) A 386.3 mm^2, N_c=75.0 kN (c) A=386.8 mm^2, N_c=75.0 kN

Figure 6: "Optimum" cross-sections for a column length of 2,500 mm, (a) fittest cross-section, (b) second fittest cross-section and (c) third fittest cross-section

Table 2 summarises the optimum average cross-sectional areas $A_{optimum}$ and axial compression capacity N_c after 10 runs. Likely due to the highly non-linear nature of the optimisation problem, the algorithm converges to slightly different cross-sectional shapes for each column length, as evident in Figure 3 through Figure 6. However, all 10 runs converge to similar values of cross-sectional areas, with coefficients of variation ranging from 0.004 to 0.008 as shown in Table 2. The algorithm accurately satisfies the targeted axial capacity of 16,861 lb (75 kN)

with a maximum average coefficient of variation and error of 0.0023 and 0.21%, respectively, for the 98.42 inches (2,500 mm) long column.

Figure 7 plots the average product between the fitness function f and $A_{squash}/A_{optimum}$ for each column length. The term $A_{squash}/A_{optimum}$ allows comparison between the fitness functions of columns of different lengths. Figure 7 shows that the algorithm converges to the "optimum" cross-sections in a relatively low number of generations, around 70 generations. Table 3 gives the main properties of the fittest cross-sections shown Figure 3 (a), Figure 4 (a), Figure 5 (a) and Figure 6 (a) for the 39.37 inches, 59.05 inches, 78.74 inches and 98.42 inches (1,000 mm, 1,500 mm, 2,000 mm and 2,500 mm) long columns, respectively.

Column length (mm)	Cross-section area ($A_{optimum}$)		Average axial capacity		
	Average (mm^2)	CoV	Average (kN)	CoV	Error (%)
1,000	242.1	0.0042	74.84	0.0023	0.21
1,500	288.7	0.0043	74.91	0.0015	0.12
2,000	337.8	0.0037	74.92	0.0013	0.11
2,500	388.4	0.0078	74.98	0.0008	0.05

Table 2: Average cross-sectional area and axial capacity at the 80th generation

Column length (mm)	A (mm^2)	I_x (mm^4)	I_y (mm^4)	C_w (mm^6)	J (mm^4)
1,000	240.5	173,055	62,273	2.511×10^8	115
1,500	287.2	286,004	112,652	6.744×10^8	138
2,000	336.8	444,174	183,051	1.460×10^9	162
2,500	385.8	705,426	277,973	2.655×10^9	185

Table 3: Main properties of the optimum cross-sections

Discussion

The cross-sections mainly converge to three different shape types, namely a "bean" shape (as in Figure 3 (a) through Figure 3 (c), or Figure 4 (c)), an "oval" shape (as in Figure 4 (a) and Figure 4 (b), Figure 5 (a) through Figure 5 (c), or Figure 6 (a)), and a rounded "Σ" shape (Figure 6). Typically, the "oval" and "bean" cross-sections are like closed profiles, whereas as the "Σ" cross-sections tend to be open. Moreover, "Σ" shape type cross-sections are generally found for the less fit cross-sections out of the 10 runs (see Savoyat et. al. (2012)), and the "oval" and "bean" cross-sections usually behave better than the "Σ" shape type cross-sections, with smaller cross-sectional areas.

The algorithm typically produces rounded cross-sectional shapes which have the advantages of (i) yielding high elastic local buckling stresses and (ii) maximising the second moments of area while minimising the cross-sectional area. Therefore, local buckling is never the dominant failure mode and the local member capacity N_{cl} is always equal to the global member capacity N_{ce} in the DSM.

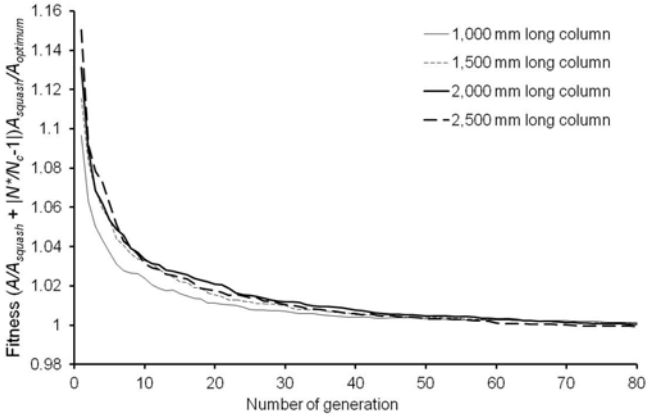

Figure 7: Evolution of the average fitness for 10 runs for each column length

Global buckling is typically the critical buckling mode for all "optimum" cross-sections with $N_c = N_{ce}$ for 38 runs out of the total 40 runs. However, the algorithm optimises for both distortional and global buckling modes and the distortional nominal capacity N_{cd} is on average equal to 17,097 lb (76.05 kN) for the 40 runs, with a coefficient of variation of 0.025, i.e. 1.4 % higher than the targeted capacity of 16,861 lb (75 kN). The close values between distortional and global buckling capacities are likely to generate buckling interaction between these two modes and therefore decrease the capacity N_c of the cross-sections (Dinis and Camotim, 2011). The distortional/global buckling interaction could be considered in the DSM by replacing the yield capacity N_y by N_{ce} in the calculation of the distortional capacity N_{cd}. (Hancock, 2007). This recommendation would result in a reduction in the axial capacity of 19.9%, 26.3%, 30.9% and 32.5% when compared to the targeted capacity of 16,861 lb (75 kN) for the 39.37 inches, 59.05 inches, 78.74 inches and 98.42 inches (1,000 mm, 1,500 mm, 2,000 mm and 2,500 mm) long columns, respectively. The distortional/global buckling interaction is therefore likely to considerably reduce the axial capacity of the cross-sections, and it is important to consider this effect (outside the scope of this paper).

Conclusions

The self-shape optimisation method was applied to strength optimisation of singly-symmetric open cold-formed steel columns The Direct Strength Method (DSM) as specified in AS/NZS 4600 Cold-formed Steel Structures was used to determine the axial member capacity N_c of the columns. Rules to automatically select the elastic local and distortional buckling stresses from the Finite Strip and constrained Finite Strip analyses have been discussed and validated against 48 conventional and 12 "optimum" cold-formed steel sections yielded in the present work. Columns with a wall thickness of 0.047 inch (1.2 mm), lengths varying from 39.37 inches to 98.42 inches (1,000 mm to 2,500 mm) and subjected to an axial compressive load of 16,861 lb (75 kN) were optimised. The cross-sections converged to "bean", "oval" or rounded "Σ" shape types, in a relatively low number of generations, around 70 generations. The rounded shapes have the advantages of increasing the local buckling strength while maximising the global buckling strength. The algorithm mainly optimises the cross-sections for distortional and global buckling, which may lead to distortional/global buckling interaction, currently not considered in the DSM.

Acknowledgment

The authors would like to thank Emeritus Professor Gregory Hancock, The University of Sydney, for his guidance in developing the automated rules.

References

Adany, S., and Schafer, B. W. (2006). "Buckling mode decomposition of single-branched open cross-section members via finite strip method: Application and examples." *Thin-Walled Structures*, 44(5), 585-600.

Adany, S., and Schafer, B. W. (2008). "A full modal decomposition of thin-walled, single-branched open cross-section members via the constrained finite strip method." *Journal of Constructional Steel Research*, 64(1), 12-29.

Adeli, H., and Cheng, N.-T. (1994). "Augmented Lagrangian Genetic Algorithm for Structural Optimization." *Journal of Aerospace Engineering*, 7(1), 104-118.

AISI (2006). *Direct Strength Method (DSM) design guide*, Washington D.C., U.S.A.

AS/NZS 4600 (2005). "Cold-formed steel structures." Standards Australia, Sydney, Australia.

BlueScope Lysaght (2009). "The Lysaght referee, 32nd Edition." BlueScope Steel Limited.

Cheung, Y. K. (1976). *Finite Strip Method in structural analysis*, Pergamon Press, Inc., New York, N.Y.

Dinis, P. B., and Camotim, D. (2011). "Post-buckling behaviour and strength of cold-formed steel lipped channel columns experiencing distortional/global interaction." *Computers & Structures*, 89(3-4), 422-434.

Gilbert, B. P., Teh, L. H., and Guan, H. (2011). "Self-shape optimisation of cold-formed steel closed profiles using Genetic Algortihm ", *Research Report CIEM/2011/R01*, Centre for Infrastructure Engineering and Management, Griffith University, Australia.

Griffiths, D. R., and Miles, J. C. (2003). "Determining the optimal cross-section of beams." *Advanced Engineering Informatics*, 17(2), 59-76.

Hancock, G. J. (1985). "Distortional buckling of steel storage rack columns." *Journal of Structural Engineering*, 111(12), 2770-2783.

Hancock, G. J. (2007). *Design of cold-formed steel structures (to AS/NZ 4600:2007) - 4th Edition*, Australian Steel Institute, North Sydney, Australia.

Holland, J. (1975). *Adaptation in Natural and Artificial Systems*, University of Michigan Press, Ann Arbor.

Leng, J., Guest, J. K., and Schafer, B. W. (2011). "Shape optimization of cold-formed steel columns." *Thin-Walled Structures*, 49(12), 1492-1503.

Li, Z., and Schafer, B. W. (2010a). "Application of the finite strip method in cold-formed steel member design." *Journal of Constructional Steel Research*, 66(8–9), 971-980.

Li, Z., and Schafer, B. W. (2010b). "Buckling analysis of cold-formed steel members with general boundary conditions using CUFSM: conventional and constrained finite strip methods." *Proc., 20th International Specialty Conference on Cold-Formed Steel Structures*

Liu, H., Igusa, T., and Schafer, B. W. (2004). "Knowledge-based global optimization of cold-formed steel columns." *Thin-Walled Structures*, 42(6), 785-801.

Savoyat, T. J.-M., Gilbert, B. P., and Teh, L. H. (2012). "Self-shape optimisation of cold-formed steel columns." *Research Report CIEM/2012/R01*, Centre for Infrastructure Engineering and Management, Griffith University, Australia.

Schafer, B. W. (2006). "Designing cold-formed steel using the direct strength method." *Proc., 18th International Specialty Conference on Cold-Formed Steel Structures*

Schafer, B. W. (2008). "Review: The Direct Strength Method of cold-formed steel member design." *Journal of Constructional Steel Research*, 64(7–8), 766-778.

Schafer, B. W., and Pekoz, T. (1998). "Direct Strength prediction of cold-formed steel members using numerical elastic buckling solutions." *Proc., 14th International Specialty Conference on Cold-Formed Steel Structures*